AIAA JOURNAL
Vol. 35, No. 6, June 1997

Vane Sweep Effects on Rotor/Stator Interaction Noise

Johan B. H. M. Schulten*
National Aerospace Laboratory NLR, 8300 AD Emmeloord, The Netherlands

The application of a lifting surface theory to compute the aerodynamic and acoustic response of swept vane stators to viscous rotor wakes is studied. Starting from the flow equations for a perturbed, axially subsonic flow, expressions are derived for the velocity field induced by a stator. A new representation of Green's function is used, which avoids the traditional expansion in duct modes. This representation is more practical for arbitrary vane shapes than the classical one. The boundary condition at the vane surfaces yields an integral equation for the unknown pressure jump distribution over the vanes. A Galerkin projection transforms this integral equation into a set of linear equations that is solved numerically. The new method agrees with the classical method and with experimental data for zero sweep. Sample calculations show that vane sweep can be exceptionally effective in the reduction of noise resulting from the interaction of rotor wakes and a stator.

Nomenclature

B	= number of blades in row considered (rotor or stator)
$\bar{c}(\rho)$	= axial extent of blade chord
$D(r)$	= angular position of zeroth vane; Eq. (10)
$\boldsymbol{g}_0(r)$	= vector normal to blade helical surface; Eq. (12)
$H_m^{(2)}$	= second kind Hankel function of order m
h	= hub/tip ratio
$\boldsymbol{i}_x, \boldsymbol{i}_r, \boldsymbol{i}_\theta$	= unit vectors in x, r, and θ directions
J_m	= Bessel function of the first kind of order m
k	= circumferential periodicity of incident velocity
M	= axial flow Mach number
$P_{\nu\lambda}$	= blade loading coefficient; Eq. (16)
p	= pressure induced by blade row
R_n	= reduced Green's function; Eq. (5)
r	= radial coordinate
t	= time coordinate
$U_{m\mu}$	= radial eigenfunction; Eq. (8)
$\boldsymbol{v}$	= velocity induced by blade row
$\boldsymbol{W}_k$	= incident velocity with circumferential periodicity k
x	= axial coordinate along duct axis
α	= axial wave number; Eq. (3)
β	= $\sqrt{(1-M^2)}$
γ	= radial wave number; Eq. (4)
Δp	= blade pressure jump distribution; Eq. (11)
$\varepsilon_{m\mu}$	= radial eigenvalue; Eq. (9)
θ	= circumferential coordinate
ξ	= axial source coordinate
ρ	= radial source coordinate
τ	= source time; Eq. (3)
ϕ	= circumferential source coordinate, local coordinate; Eq. (15)
Ω	= tangential tip Mach number
$\langle\,\rangle$	= inner product of three-dimensional vectors

Subscripts

L	= leading edge
T	= trailing edge

Superscripts

(a)	= anechoic
$+$	= blade lower side
$-$	= blade upper side
$\hat{(\,)}$	= in physical domain

Received March 25, 1996; presented as Paper 96-1694 at the CEAS/AIAA 2nd Aeroacoustics Conference, State College, PA, May 6–8, 1996; accepted for publication Feb. 20, 1997.

*Senior Research Engineer, Aeroacoustics Department, P.O. Box 153. E-mail: schulten@nlr.nl. Senior Member AIAA.

Introduction

THE interaction of fan wakes and stator outlet guide vanes is the major fan noise mechanism in current high, and future very high, bypass turbofan engines. To reduce interaction noise, active means have been investigated extensively in recent years.[1] Although some solutions are quite promising, active suppression almost invariably implies delicate and expensive control systems.

By comparison, passive concepts are relatively simple, and some of them, such as acoustic duct lining, already have been applied for a long time. With regard to fan geometry the most famous design rule is Tyler and Sofrin's selection criterion[2] for blade and vane numbers, which is used to achieve a cut-off blade passing frequency in modern fan designs. A large axial gap between fan and outlet guide vanes is also widely appreciated as an effective method of passive noise control. A more sophisticated passive way is to exploit rotor shielding to reflect most of the upstream propagating sound.[3] It is obvious that substantial shielding can only be expected when rotor and acoustic mode rotate in an opposite way. An accurate calculation of the magnitude of this effect requires a method at least at the level of the lifting surface approximation.[4] For the sound propagating downstream from the outlet guide vanes, the absence of such shielding is a matter of increasing concern with regard to the emerging very high bypass fans.

In a more general sense, passive noise control is equivalent to the design of inherently quiet fans. Therefore, it requires a fairly complete modeling of the sound generation process. Calculation is necessary since intuition easily fails, as was shown for leaned vanes,[5] which seem not to provide a viable way to sound reduction for low circumferential mode number of the generated sound.

Vane sweep has been recognized as a potential sound reducing measure for a long time[6] and is used in several current fan designs. An early study relevant to vane sweep was made by Adamcyk,[7] who analyzed the interaction of an oblique gust with a semi-infinite, swept plate. His analysis showed that the resulting sound is cut-off, i.e., not radiating, if the phase velocity of the interaction along the leading edge is subsonic. The latter can be achieved by applying sufficient sweep. Adamcyk's model[7] was extended by Envia and Kerschen[8] to include finite span and planar cascade effects. These models are essentially high-frequency approximations, which are of lasting value because other, more complete methods become computationally inefficient or even fail for very high frequencies. For the calculation of the intermediate-frequency interaction sound, lifting surface methods for finite chord blades in annular ducts have been shown to be very useful.[9–13] However, it was not until 1989 that an unsteady lifting surface method for a rotor with swept blades was published, by Kodama and Namba.[14] They found favorable effects of blade sweep on the acoustic response to sinusoidal gust

interaction. However, to reduce interaction noise it is more natural to look at the stator vanes, which also have less structural constraints than rotor blades.

Lifting surface methods have the outstanding advantage of being fully consistent with the level of approximation of linear duct acoustics, still the favored model for high-frequency acoustic lining optimization. Also, the physically important ratio of blade row dimensions and the acoustic and hydrodynamic wavelengths involved is conserved in the lifting surface approximation.

Compared to Euler and Navier–Stokes methods, the absence of numerical dissipation or dispersion in the lifting surface methods, their exactness, and their, by comparison, short computation times make them very suitable for optimization of blade and vane geometries. They also can provide limiting test cases with which to compare results of numerical methods. A further advantage is that, by their analytical nature, in general, isolated effects can be traced more precisely. A drawback may be the mathematical complexity of the formulations and, of course, their inherent limitation to small perturbations.

The basic result of any lifting surface method is the pressure jump distribution over the blades or vanes. Once the pressure jump distribution is known, it is only a minor effort to compute the steady and unsteady pressure or velocity fields generated by the blade row. In the present paper a lifting surface method is applied to swept stator vanes. The method is based on a new representation of the Green's function,[15] which is basically an extension of the Fourier expansion of the free-space Green's function for propellers to include the sound reflections by hub and casing. The method is validated with experimental results of the National Aerospace Laboratory NLR (NLR) rotor/stator interaction model[16] and with results of the classical method for unswept vanes. For this configuration the effects of a progressive vane sweep angle on the first and second harmonic of the interaction sound are studied. The numerical accuracy of the method is checked by varying the number of basis functions that describe the vane pressure jump distribution. Further, the potential of vane sweep for a typical high-speed fan geometry is numerically explored.

Analysis

Governing Equations

A lifting surface modeling of a flow problem is based on two assumptions. First, the viscosity of the flow is considered to be small, i.e., the Reynolds number is assumed to be sufficiently high. Second, the perturbations of the main flow caused by the presence of the blades are supposed to be relatively small.

We consider a single blade row placed in a uniform, subsonic main flow of Mach number $M(0 < M < 1)$. To obtain a nondimensional formulation, the mass density and speed of sound of the main flow and the duct radius are taken as scaling parameters. With this scaling, the pressure and density perturbation become to leading order identical. If the x axis is chosen along the duct axis, the governing, i.e., the leading order, flow equations are the linearized Euler equations for the (dimensionless) perturbation pressure $\tilde{p}$ and velocity $\tilde{\boldsymbol{v}}$:

$$\frac{\mathrm{D}\tilde{p}}{\mathrm{D}t} + \langle \nabla \cdot \tilde{\boldsymbol{v}} \rangle = 0 \tag{1}$$

and

$$\frac{\mathrm{D}\tilde{\boldsymbol{v}}}{\mathrm{D}t} + \nabla \tilde{p} = \boldsymbol{0} \tag{2}$$

where the linearized material derivative $\mathrm{D}/\mathrm{D}t = \partial/\partial t + M\partial/\partial x$. A tilde indicates that the variable is understood to be in the physical domain.

As shown previously,[17,18] application of generalized functions to make Eqs. (1) and (2) formally valid throughout space, i.e., also within the blades, and elimination of the velocity yield a nonhomogeneous convected-wave equation in the pressure. The right-hand side of this equation consists of two source terms, one of which contains the blade loading distribution and the other the blade thickness distribution. After the construction of a Green's function for this equation in terms of a multiple Fourier transform, the pressure field of the complete blade row can be expressed as an integral over a volume that contains the blade row. This pressure field contains both steady and unsteady, acoustic components at multiples, including zero, of the blade passing frequency. Upon substitution of the pressure field, the momentum equation yields expressions for the velocity induced by blade displacement and the blade loading velocity.

Green's Function

In this section we will construct $\tilde{G}$ as the superposition of Green's function in free space and cylindrical waves reflected by the hub and the casing. This is possible by representing $\tilde{G}$ as a superposition of circumferential and axial waves in the following multiple wave spectrum:

$$\tilde{G}(x, r, \theta, t \mid \xi, \rho, \phi, \tau) = \frac{1}{(2\pi)^3} \sum_{n=-\infty}^{\infty} \exp[in(\theta - \phi)] \times \int_{-\infty}^{\infty}\int_{-\infty}^{\infty} \exp\{i[\omega(t-\tau) + \alpha(x-\xi)]\} R_n(\alpha, r, \omega \mid \rho)\, \mathrm{d}\alpha\, \mathrm{d}\omega \tag{3}$$

where R_n is a reduced Green's function, defined subsequently. In this formulation chordwise integrals can be easily taken because the axial source coordinate ξ only occurs directly in an exponential. Now we introduce the radial wave number γ, which is related to the axial wave number α and the Helmholtz number (dimensionless frequency) ω as

$$\gamma^2 = (\omega + M\alpha)^2 - \alpha^2 \tag{4}$$

If the branch cuts of γ are taken such that $\mathrm{Im}\ \gamma \leq 0$ throughout the complex α plane, the anechoic, free space reduced Green's function is given by[15]

$$R_n^{(a)} = -i(\pi/2)\left[J_n(\gamma r) H_n^{(2)}(\gamma\rho) H(\rho - r) + J_n(\gamma\rho) H_n^{(2)}(\gamma r) H(r - \rho)\right] \tag{5}$$

where H denotes the Heaviside unit step function. In the present case of a cylindrical duct, the hard wall boundary condition $\partial R_n/\partial r = 0$ at the hub ($r=h$) and at the casing ($r=1$) is satisfied by adding the reflected cylindrical waves. Therefore, we presume

$$R_n = R_n^{(a)} + AH_n^{(2)}(\gamma r) + BJ_n(\gamma r) \tag{6}$$

Because the added cylindrical waves satisfy the Bessel equation, they do not affect the right-hand side in the equation for the Green's function.[15] Application of the boundary conditions at hub and casing determines the coefficients A and B, and we obtain

$$R_n = R_n^{(a)} + i\frac{\pi}{2}\frac{1}{J_n'(\gamma) H_n^{(2)\prime}(\gamma h) - J_n'(\gamma h) H_n^{(2)\prime}(\gamma)} \times \left\{\left[J_n'(\gamma) H_n^{(2)}(\gamma\rho) - H_n^{(2)\prime}(\gamma) J_n(\gamma\rho)\right] J_n'(\gamma h) H_n^{(2)}(\gamma r) - \left[J_n'(\gamma h) H_n^{(2)}(\gamma\rho) - H_n^{(2)\prime}(\gamma h) J_n(\gamma\rho)\right] H_n^{(2)\prime}(\gamma) J_n(\gamma r)\right\} \tag{7}$$

The reason to avoid the more natural combination of Hankel functions of the first and second kind in Eq. (6), or, alternatively, the Bessel functions of the first and second kind, is that this would lead to subtraction of very large terms in certain parts of the α plane with subsequent fatal loss of numerical accuracy. It is noted that R_n has a finite limit for $|\gamma| \to 0$, which is obtained by substituting the ascending series for J_n and $H_n^{(2)}$ in Eqs. (5) and (7).

After rearrangement of Eq. (7) it is possible to recover the traditional Green's function by performing the Fourier integral to α, which comes down to summation of the residues. Then the classical Green's function representation in duct modes given by

$$\tilde{G} = \frac{1}{(2\pi)^2}\int_{-\infty}^{\infty} \exp[i\omega(t-\tau)] \sum_{n=-\infty}^{\infty} \exp[in(\theta-\phi)] \sum_{\mu} U_{n\mu}(r) \times \frac{U_{n\mu}(\rho)}{2i\beta_{n\mu}(\omega)} \exp\left\{i\frac{(x-\xi)}{\beta^2}[M\omega - \mathrm{sgn}(x-\xi)\beta_{n\mu}(\omega)]\right\} \mathrm{d}\omega \tag{8}$$

results. Here the square root $\beta_{n\mu}$ is defined as

$$\begin{aligned} \beta_{n\mu} &= \omega\sqrt{1-(\varepsilon_{n\mu}\beta/\omega)^2} \qquad \text{if} \qquad (\varepsilon_{n\mu}\beta)^2 \le \omega^2 \\ \beta_{n\mu} &= -i\sqrt{(\varepsilon_{n\mu}\beta)^2-\omega^2} \qquad \text{if} \qquad (\varepsilon_{n\mu}\beta)^2 > \omega^2 \end{aligned} \tag{9}$$

where the radial eigenvalues are denoted by $\varepsilon_{n\mu}$. It is noted that the zeros of the denominator of Eq. (7) in the complex α plane are the modal eigenvalues $\varepsilon_{n\mu}$.

An advantage of using Fourier–Bessel expansions as Eqs. (3) and (8) for the Green's function is the fact that the composing terms are continuous functions, also in the source point. A disadvantage is the complexity of the multiple, nested series and integrals. Note that the expansions do not have a pointwise convergence, but only represent the Green's function in a generalized sense. In the final results, however, the Green's function will appear only in integrals over a blade surface. After taking these integrals inside, the resulting expansion, in general, converges slowly. To accelerate the convergence, special techniques,[19] such as Euler summation of the oscillating tails of the α integral and Richardson extrapolation of the n-series, are applied in the numerical evaluation.[15]

Not only Green's function, but any sound field in a duct, can be described in terms of a superposition of duct modes. If $\beta_{n\mu}(\omega)$ is real, the mode is said to be cut-on because it propagates without attenuation along the duct in the upstream and downstream directions. If, on the other hand, $\beta_{n\mu}(\omega)$ is imaginary, the mode is cut-off because it is exponentially decaying from the source. Each mode has its particular cut-off frequency given by $\pm\beta\varepsilon_{n\mu}$. This classical representation of Green's function has been used in all lifting surface methods for ducted fans thus far. Its main disadvantage is the partly highly damped and partly highly oscillating character of the large-order eigenfunctions $U_{n\mu}$ (Fig. 1), which leads to a cumbersome numerical integration in the blades spanwise direction, because asymptotic integration techniques,[19] such as the method of stationary phase, cannot uniformly be applied. Furthermore, the expansion of Eq. (8) cannot be used for incident distortion fields at a cut-off frequency of one of the duct modes. By virtue of using a deformed contour to perform the α integral, the expansion of Eq. (3) can still be used.

Until recently,[14] the traditional expansion of Green's function into duct modes[9–12] has only been applied to ducted blade rows of the most simple geometry, i.e., leading and trailing edges in cross-sectional planes. The reason for this is that the infringement on the separation of variables by swept or tapered blades increases the complexity as well as the computational effort dramatically. If only the field upstream or downstream of a blade row is to be described, the classical Green's function is the more efficient vehicle. Then, the complete sound field in a duct can be described to high accuracy by a relatively small number of duct modes, namely, the cut-on modes supplemented with a few cut-off modes. However, in a lifting surface problem high-order cut-off modes play a much more important role than they do at some axial distance from the blade row. The present formulation [Eq. (3)], in which the summation over radial modes has been replaced by an integral, accepts blades of a general planform, i.e., with leading and trailing edges that are a function of the radius, without significant penalty in complexity. Therefore, it seems much better suited to study effects such as blade sweep and taper on the sound generation process of ducted fans.

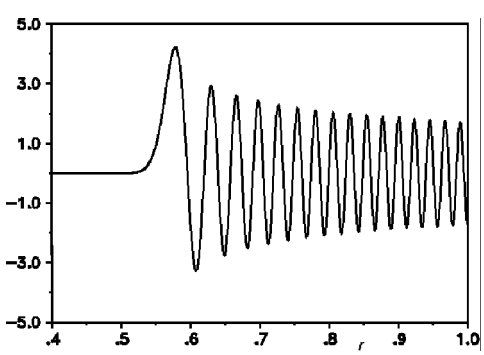

Fig. 1 Example of radial eigenfunction $U_{n\mu}(r)$; $n = 200$, $\mu = 32$, and $h = 0.4$.

Blade Loading Velocity Field

As shown in Ref. 15, substitution of the actual force field exerted by the blades into the expression for the velocity leads, after some algebra, to the following expression for the velocity induced by a blade row:

$$\begin{aligned} \tilde{\boldsymbol{v}}_F = \frac{B}{(2\pi)^3 M} \sum_n \sum_{-\infty}^{\infty} \int_{-\infty}^{\infty} \exp(i\omega_n t)\exp(im\theta) \\ \times \int_{-\infty}^{\infty} \frac{\exp(i\alpha x)}{i[\alpha+(\omega_n/M)]} \int_h^1 \rho \exp[-imD(\rho)] \left\{ \boldsymbol{g}_0(\rho)\frac{\delta(r-\rho)}{r} \right. \\ \left. - \begin{bmatrix} \alpha \\ -i\partial/\partial r \\ m/r \end{bmatrix} \left\langle \boldsymbol{g}_0(\rho) \,\middle|\, \begin{bmatrix} \alpha \\ i\partial/\partial\rho \\ m/\rho \end{bmatrix} \right\rangle R_m(\alpha, r, \omega_n \,|\, \rho) \right\} \\ \times \int_{x_L(\rho)}^{x_T(\rho)} \exp\left[i\left(\frac{m\Omega}{M} - \alpha \right)\xi \right] \Delta p(\xi, \rho, \omega)\, d\xi\, d\rho\, d\alpha\, d\omega \end{aligned} \tag{10}$$

where $\omega_n = \omega - m\Omega$ and $m = k - nB$. Note that k denotes the full circumferential periodicity of the incident field, regardless of its origin. Similarly, B always denotes the number of blades in the exposed blade row, irrespective of being a rotor or a stator. For the sake of completeness this expression is for a rotor. For a stator it simplifies because then $\Omega = 0$. The pressure jump distribution is defined as

$$\Delta p(\xi, \rho, \omega) = p^+(\xi, \rho, \omega) - p^-(\xi, \rho, \omega) \tag{11}$$

and the vector normal to the undisturbed helical surfaces

$$\boldsymbol{g}_0(r) = (\Omega/M)\boldsymbol{i}_x - D\prime(r)\boldsymbol{i}_r + (1/r)\boldsymbol{i}_\theta \tag{12}$$

For stator vanes without lean, a further simplification is that $D\prime = 0$ in Eq. (12).

Equation (10) contains both the vortical and the irrotational (i.e., associated with the pressure waves) velocity field. The vortical field results both from the first and the second term in braces, whereas the irrotational field results from the second term only. By taking a contour integral in the α plane it can be readily verified that the first term yields a Heaviside function in $(x - \xi)$ with a streamwise Strouhal periodicity. The second term also yields such a field plus a modal wave system similar to that of the Green's function in Eq. (8).

Integral Equation

The only unknown quantity in the expression of the blade loading velocity [Eq. (10)] is the blade pressure jump distribution Δp. To solve Δp we have to apply the boundary condition of flow tangency at the blade surfaces. This boundary condition is rewritten in such a way that the right-hand side depends solely on known quantities. By splitting the incident field into circumferential Fourier components $\tilde{\boldsymbol{W}}_k(x, r, t)\exp(ik\theta)$, the integral equation has to be solved for one blade only. Combining the boundary conditions at upper and lower blade surfaces, as in Ref. 15, we obtain the following integral equation for Δp due to an incident velocity field:

$$\left[\left\langle \boldsymbol{g}_0 \cdot \tilde{\boldsymbol{v}}_F \right\rangle = -\left\langle \boldsymbol{g}_0 \cdot \tilde{\boldsymbol{W}}_k e^{ik\theta} \right\rangle \right]_{\theta = D + \Omega(t - x/M)} \tag{13}$$

Taking the Fourier transform in time of both sides of Eq. (13) permits the solution of the problem per frequency ω

Numerical Solution Procedure

The first step toward the numerical solution of the integral equation [Eq. (13)] is the choice of a suitable description of the unknown pressure jump distribution. In principle, this can be achieved by approximating Δp by a finite set of basis functions, also called loading or trial functions. Because vanes operate definitely in the subsonic regime, an appropriate choice for the chordwise representation is[15]

$$\Delta p = P_0(\rho)\tan\frac{\phi}{2} + \sum_{\lambda}^{\lambda_{\max}} P_\lambda(\rho)\sin\lambda\phi \tag{14}$$

where ξ is related to ϕ by

$$\xi = \frac{x_T(\rho) + x_L(\rho)}{2} + \frac{\bar{c}(\rho)}{2}\cos\phi \tag{15}$$

This representation incorporates the usual subsonic square root leading-edge singularity, as well as a Kutta condition behavior at the trailing edge. It also permits the chordwise integrals in Eq. (10) to be evaluated analytically, a most welcome computer time saving quality, which is missed with the classical Green's function representation.

In the spanwise direction $P_\lambda(\rho)$ is expanded in a Chebyshev series as follows:

$$P_\lambda(\rho) = \sum_{\nu=0}^{\nu_{\max}} P_{\nu\lambda}\cos\nu\psi \tag{16}$$

where

$$\cos\psi = 2(\rho - h)/(1 - h) - 1 \tag{17}$$

Now a Galerkin projection, as described in Ref. 20, transforms the integral equation into a system of linear equations that can be solved by standard matrix techniques.

Experimental Validation

To validate the new method, it was applied to a standard experimental NLR test case. Figure 2 shows the experimental model[13,16] consisting of a through-flow nacelle with a 0.4-m-diam duct, which was installed in a low-speed wind tunnel. A 0.24-m-diam hub formed the inner boundary of the annular geometry in which a stator with 18 unswept vanes was installed. In front of the stator, a rotor consisting of 16 cylindrical rods (3 mm diam) was mounted. These rods were used as acoustically transparent wake generators to produce a periodic velocity perturbation field.

The comparison of the new lifting surface method and the classical one for the NLR fan experiment is made in Fig. 3. Obviously the absolute values of the pressure jump distributions of both lifting surface methods are close, with the classical one showing a slightly larger discrepancy with the experiment. Note that differences between the two methods are entirely due to differences in the numerical treatment and subsequent programming, because the

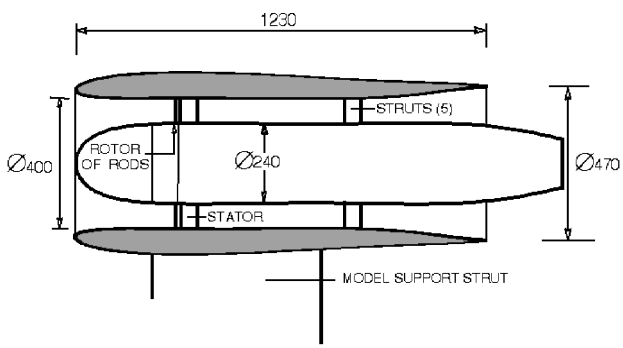

Fig. 2 NLR fan noise wind-tunnel model (dimensions in millimeters).

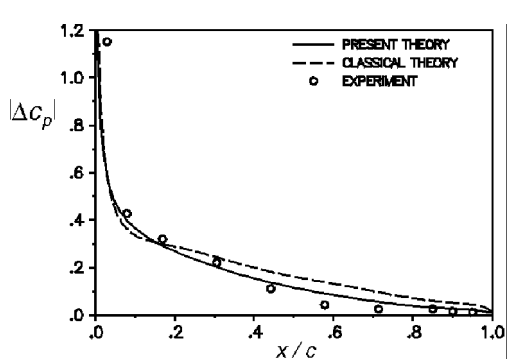

Fig. 3 Comparison of two lifting surface methods with NLR fan experiment[13]: first harmonic, $r = 0.8$ (midspan), conditions in Table 1.

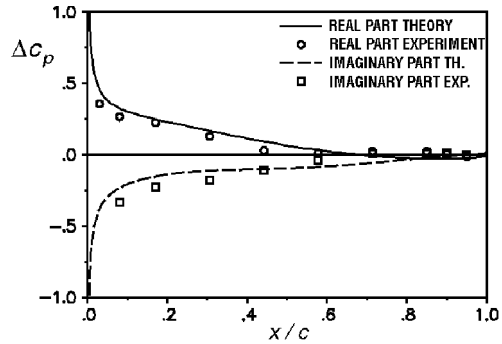

Fig. 4 Midspan pressure jump distribution; first harmonic, conditions in Table 1.

methods are analytically equivalent. The agreement with the experiment is surprisingly good, bearing in mind that in this case the disturbance level is as high as 20% of the freestream velocity, which can be hardly considered to be a small perturbation. Figure 4 shows a complex representation of the pressure jump distribution, measured and computed with the present theory. It also appears that the phase is accurately predicted. For this comparison use was made of the measured wake velocities to obtain the right-hand side of Eq. (13). It was found that Schlichting's wake formulas[21] give a good description of these wakes. Therefore, these formulas were used in the next numerical examples for swept vanes.

Numerical Examples

Low-Speed Configuration

The NLR fan experiment was taken as a starting point for an exploratory study of the effects of vane sweep. For the first harmonic of the rod wake system, lifting surface calculations were made for sweep angles up to 30 deg at 5-deg intervals. The vane intersection with the hub was kept in place while the intersection with the casing followed from the sweep angle (Fig. 5 and Table 1). This way the vane area was kept constant.

First Harmonic

Figure 6 shows the first harmonic upstream and downstream acoustic intensity level in decibels (referred to 10^{-12} W/m^2). Because in this case only one mode is cut-on at the first harmonic ($m = 2$, $\mu = 1$), this is also the modal intensity. Clearly, the upstream power virtually disappears beyond 20 deg of sweep. The downstream power falls slower but at a sweep angle of 30 deg also, the downstream power has effectively vanished.

The difference in upstream and downstream behavior is a consequence of the difference in the modal axial wavelength, as can be seen in the expression for the pressure induced by the loading of an unleaned vane:

$$\tilde{p}_F(x, r, \theta, t) = \frac{-B}{2\pi}\exp(i\omega t)\sum_{m=-\infty}^{\infty}\exp[im(\theta - D)]$$
$$\times\sum_{\mu=0}^{\infty}\frac{U_{m\mu}(r)}{2\beta_{m\mu}(\omega)}\int_h^1\frac{m}{\rho}U_{m\mu}(\rho)\int_{x_L(\rho)}^{x_T(\rho)}\exp\left\{i\frac{(x-\xi)}{\beta^2}[M\omega - \mathrm{sgn}(x-\xi)\beta_{m\mu}(\omega)]\right\}\Delta p(\xi,\rho)\,\mathrm{d}\xi\,\mathrm{d}\rho \tag{18}$$

In the present case $\beta_{2,1} = 6.015$, which yields an upstream wave number of 7.599 and a downstream wave number of -4.431. Because these wave numbers occur also in the exponential in the chordwise integral in Eq. (18), it may be clear that the upstream mode is almost twice as sensitive to an axial source variation as the downstream mode. Thus, it is to be expected that the upstream mode more directly responds to vane sweep than the downstream mode with its longer wavelength.

It is observed that the downstream level is considerably higher than the upstream level. Because the upstream propagating sound can also be reduced by rotor shielding, it is the downstream sound that would need all the attention in this case. It is obvious that

Table 1 Low-speed configuration

Number of rotating rods	16
Number of stator vanes	18
Hub/tip ratio h	0.6
Axial vane chord length	0.25
Axial Mach number	0.244
Rods circumferential tip Mach number	0.406
Rods drag coefficent	1.2
Nondimensional first harmonic frequency	6.491
Speed of sound, m/s	340.43
Air density, kg/m^3	1.225

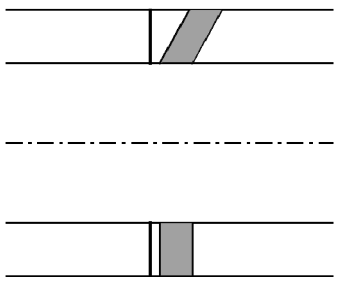

Fig. 5 Low-speed interaction model with rotating rods and unswept vanes (lower) and 30-deg swept vane configuration as computed (upper); conditions in Table 1.

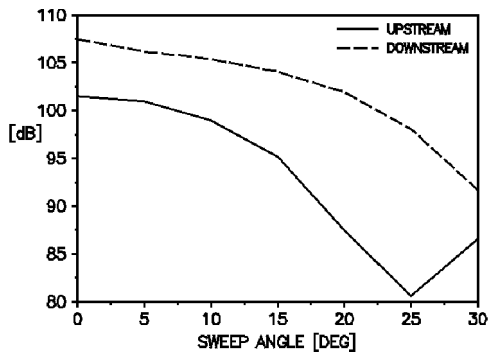

Fig. 6 Acoustic intensity level first harmonic; conditions in Table 1.

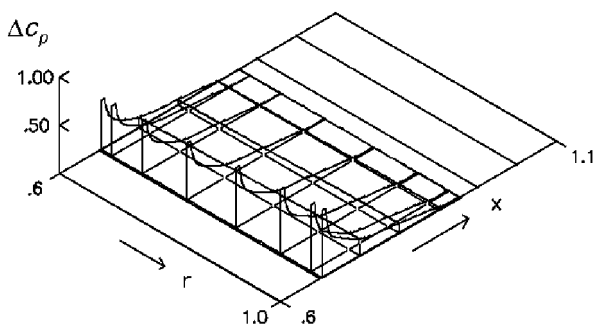

Fig. 7a Real part of pressure jump distribution for 0 deg of sweep, first harmonic; conditions in Table 1.

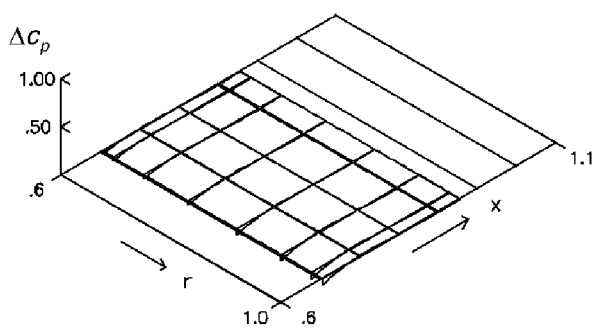

Fig. 7b Imaginary part, 0 deg of sweep.

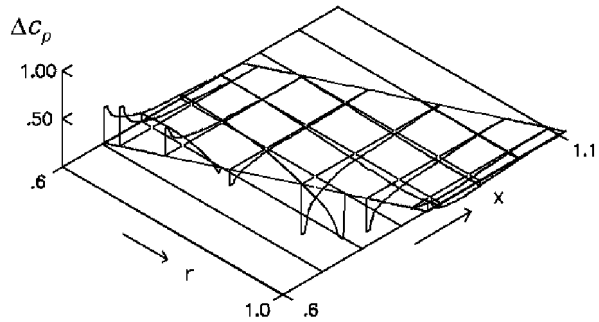

Fig. 8a Real part of pressure jump distribution for 25 deg of sweep, first harmonic; conditions in Table 1.

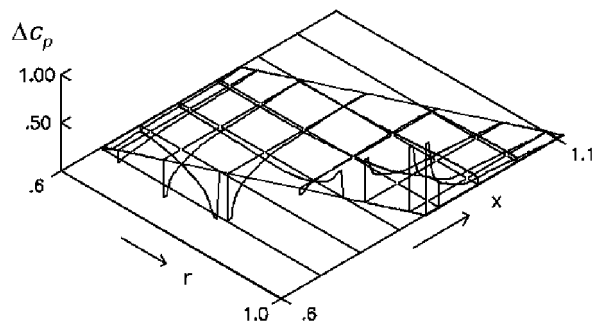

Fig. 8b Imaginary part, 25 deg of sweep.

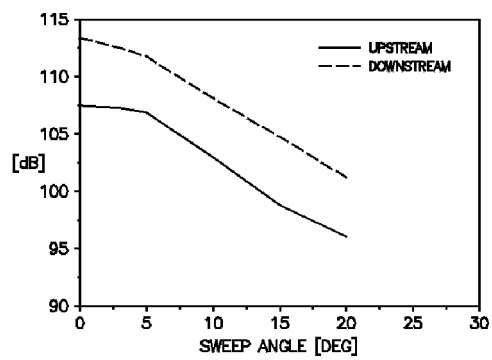

Fig. 9 Acoustic intensity level second harmonic; conditions in Table 1.

impressive sound reductions of more than 15 dB can be achieved both upstream and downstream, even with a simple constant sweep angle. Note that the reduction is of the same order as that recently reported by Kerschen and Reba[22] for active control leading-edge actuators.

To show that the noise reduction is not caused by a vanishing aerodynamic response, the pressure jump distributions for 0 and 25 deg of sweep are shown in Figs. 7a and 7b and 8a and 8b, respectively. Obviously, the pressure jump does not vanish at all for 25 deg of sweep but shows a strong spanwise phase variation compared to the 0-deg sweep case. Thus, the primary effect of sweep is to promote a poor coupling between blade loading and propagating acoustic modes.

Second Harmonic

In Fig. 9 the results for the second harmonic are shown. At this frequency two modes with circumferential periodicity $m = 4$ are cut-on. For the upstream power it takes about 5 deg of sweep before it starts to fall. The downstream intensity directly starts to decrease but beyond 15 deg the upstream and downstream sound reductions are practically equal. A 10-dB reduction is attained at 20 deg. Note that the overall intensity level sound is higher than it was for the first harmonic. Also, the downstream level is again considerably higher than the upstream.

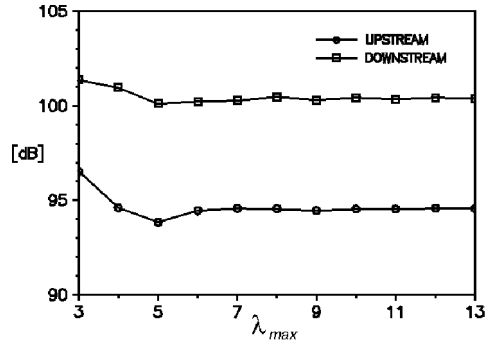

Fig. 10 Effect of the number of chordwise basis functions, sweep angle 20 deg, $\nu_{max} = 10$, second harmonic; conditions in Table 1.

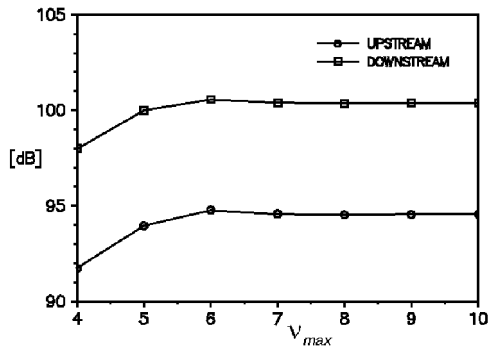

Fig. 11 Effect of number of spanwise basis functions, sweep angle 20 deg, $\lambda_{max} = 13$, second harmonic; conditions in Table 1.

Numerical Validation of Method

To check the numerical accuracy of the method, the number of basis functions representing the pressure jump distribution was systematically varied. The number of basis functions strongly affects the required computing time and normally one should avoid an overdose of basis functions. The second harmonic of the low-speed case just discussed was used as a test case. A typical computing time for one sweep angle of this case is 24 h on a Pentium 133 system, whereas higher harmonics are even more demanding. Figure 10 presents the computed intensity level for a sweep angle of 20 deg as a function of the number of chordwise basis functions. The number of spanwise basis functions was kept constant at 11 ($= \nu_{max} + 1$). It appears that beyond $\lambda_{max}=6$ the computed intensity level is practically constant.

The same exercise was done for the spanwise basis functions while the number of chordwise functions was kept at 14 ($= \lambda_{max}+1$). From Fig. 11, it is clear that $\nu_{max} = 7$ is sufficient for a correct result.

These figures are very much case related. In particular, a different frequency, chord length, and hub/tip ratio h will change the minimum required number of basis functions.

High-Speed Fan

Although the previous example had the advantage of a direct relation to a well-documented experiment, the real interest of the method is, of course, in its application to the emerging very high bypass turbofans. Inspired by the advanced ducted propeller (ADP) experiment by Woodward et al.,[23] a high-speed fan configuration was defined, as given in Table 2 and Fig. 12. As usual for modern fans, the first harmonic is cut-off. In the second harmonic four modes with circumferential periodicity $m = 8$ are cut-on. The nondimensional frequency of this case is almost twice as high as in the earlier example.

The rotor chord was taken as

$$c(r) = 0.247\sqrt{1 + [(2r/(1+h)]^2} \tag{19}$$

With a constant rotor blade drag coefficient of 0.01, the turbulent, viscous wakes were computed in a quasi-two-dimensional way[15,21] to provide the incident velocity field in Eq. (13). To keep the average gap between rotor and stator constant, in the present example the midspan leading-edge point was held in place as the sweep angle was varied (Fig. 12). Here, the axial gap itself was taken smaller than would be typical in an actual ADP design to prevent a completely merged viscous wake system with a rather unpredictable residual structure. It may be expected that for a large gap it is the inviscid wake system of the fan that dominates the incident velocity field at the vanes. The present viscous wake system, therefore, should be considered only as a sample to demonstrate the effect of vane sweep for a well-organized incident field.

Table 2 High-speed fan example

Number of rotor blades	16
Number of stator vanes	40
Hub/tip ratio h	0.45
Initial vane chord length	0.17
Mid span axial gap	0.219
Axial Mach number	0.288
Rotor circumferential tip Mach number	0.76
Rotor blade drag coefficient	0.01
Nondimensional second harmonic frequency	24.32
Speed of sound, m/s	340.43
Air density, kg/m^3	1.225

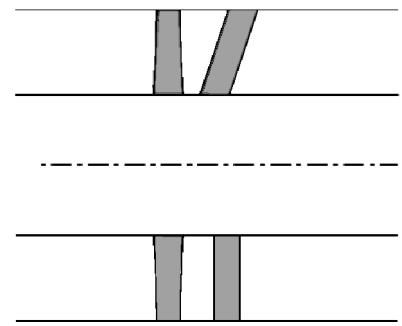

Fig. 12 High-speed fan geometry: 20-deg swept vane (upper) and unswept vane (lower); also see Table 2.

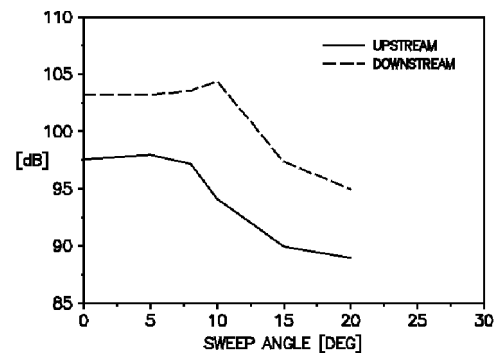

Fig. 13 Acoustic intensity level, second harmonic; conditions in Table 2.

Another point of concern is the loss of steady aerodynamic loading of a swept vane. For a high aspect ratio vane the aerodynamic performance depends on the velocity component normal to the leading edge rather than on the total velocity. To preserve the aerodynamic performance, the axial vane chord was varied with the sweep angle as

$$c = \frac{c_0}{\cos^2 \lambda} \tag{20}$$

where c_0 is the initial chord at zero sweep and λ is the sweep angle. As a result, the vane surface also increases with the sweep angle (Fig. 12).

It is shown in Fig. 13 that sweep does not yield immediate benefits for this configuration. On the contrary, first some critical value has to be passed before a sharp decrease begins. The upstream sound starts to decrease earlier than the downstream sound, which requires about 12 deg to become lower than its zero sweep level. Thus, a too

small sweep angle may have an adverse effect. Still considerable sound reductions on the order of 8 dB are possible with 20 deg of sweep. The downstream intensity level is again considerably higher than the upstream level.

Concluding Remarks

The application of a lifting surface method to the calculation of aerodynamic and acoustic response of swept stators to impinging rotor wakes has been discussed. A new element in the present method is the representation of the Green's function as an integral instead of the more familiar infinite sum of radial modes. The method can be considered as an extension of a propeller lifting surface formulation.

Comparison with experimental data and results of the classical Green's function formulation shows the validity of the new method. The numerical consistency of the method has been checked by systematically varying the representation of the unsteady vane pressure jump distribution.

Calculations for the experimental NLR fan model for a range of sweep angles up to 30 deg show a potential of 10–15 dB noise reduction.

At conditions relevant for a modern, very high bypass design, interaction noise reductions of the order of 8 dB seem to be obtainable with 20 deg of vane sweep. Smaller sweep angles may cause a sound increase.

The found effectiveness of a simple backward vane sweep invites to further research into forward sweep and more sophisticated, curved vane planforms.

For the same sweep angle, the computed downstream noise levels persistently appear to be considerably higher than upstream levels.

References

[1]Simonich, J. C., "A Review of Actuators for Active Noise Control in Gas Turbines," *Proceedings of the 1st Joint CEAS/AIAA Aeroacoustics Conference* (Munich, Germany), Vol. 1, Deutsche Gesellschaft fuer Luft- und Raumfahrt, Bonn, Germany, 1995, pp. 445–453.

[2]Tyler, J. M., and Sofrin, T. G., "Axial Flow Compressor Noise Studies," *SAE Transactions*, Vol. 70, 1962, pp. 309–332.

[3]Smith, M. J. T., *Aircraft Noise*, Cambridge Univ. Press, New York, 1989.

[4]Schulten, J. B. H. M., "Transmission of Sound Through a Rotor," *Proceedings DGLR/AIAA 14th Aeroacoustic Conference* (Aachen, Germany), Vol. 1, Deutsche Gesellschaft fuer Luft- und Raumfahrt, Bonn, Germany, 1992, pp. 502–509.

[5]Schulten, J. B. H. M., "Sound Generated by Rotor Wakes Interacting with a Leaned Vane Stator," *AIAA Journal*, Vol. 20, No. 10, 1982, pp. 1352–1358.

[6]Hayden, R. E., Bliss, D. B., Murray, B. S., Chandiramani, K. L., Smullin, J. I., and Schwaar, P. G., "Analysis and Design of a High Speed, Low Noise Aircraft Fan Incorporating Swept Leading Edge Rotor and Stator Blades," NASA CR 135092, Dec. 1977.

[7]Adamcyk, J. J., "Passage of a Swept Airfoil Through an Oblique Gust," *Journal of Aircraft*, Vol. 11, No. 5, 1974, pp. 281–287.

[8]Envia, E., and Kerschen, E. J., "Noise Generated by Convected Gusts Interacting with Swept Airfoil Cascades," AIAA Paper 86-1872, July 1986.

[9]Namba, M., "Three-Dimensional Analysis of Blade Force and Sound Generation for an Annular Cascade in Distorted Flows," *Journal of Sound and Vibration*, Vol. 50, No. 4, 1977, pp. 479–508.

[10]Kobayashi H., and Groeneweg, J. F., "Effects of Inflow Distortion Profiles on Fan Tone Noise," *AIAA Journal*, Vol. 18, No. 8, 1980, pp. 899–906.

[11]Lordi, J. A., and Homicz, G. F., "Linearized Analysis of the Three-Dimensional Compressible Flow Through a Rotating Annular Blade Row," *Journal of Fluid Mechanics*, Vol. 103, 1981, pp. 413–442.

[12]Salaün, P., "Unsteady Aerodynamic Pressures on an Annular Cascade in Subsonic Flow," ONERA Publ. No. 158, May 1974 (in French); translated into English as European Space Agency Tech. Transl., ESA-TT-173, 1975.

[13]Schulten, J. B. H. M., "Experimental Validation of a Lifting Surface Model for Rotor Wake–Stator Interaction," AIAA Paper 89-1125, April 1989.

[14]Kodama, H., and Namba, M., "Unsteady Lifting Surface Theory for a Rotating Cascade of Swept Blades," American Society of Mechanical Engineers, ASME Paper 89-GT-306, June 1989.

[15]Schulten, J. B. H. M., "Sound Generation by Ducted Fans and Propellers as a Lifting Surface Problem," Ph.D. Thesis, Dept. of Applied Mathematics, Univ. of Twente, Enschede, The Netherlands, Feb. 1993.

[16]Zandbergen, T., "Stator Vane Response Due to the Impingement of the Wake of an Unloaded Rotor," AIAA Paper 88-2814, July 1988.

[17]Schulten, J. B. H. M., "Effects of Asymmetric Inflow on Near-Field Propeller Noise," *AIAA Journal*, Vol. 34, No. 2, 1996, pp. 251–258.

[18]Ffowcs Williams, J. E., and Hawkings, D. L., "Sound Generation by Turbulence and Surfaces in Arbitrary Motion," *Philosophical Transactions of the Royal Society of London*, Series A, Vol. 264, 1969, pp. 321–341.

[19]Bender, C. M., and Orszag, S. A., 1978, *Advanced Mathematical Methods for Scientists and Engineers*, McGraw–Hill, New York, Chaps. 6 and 8.

[20]Schulten, J. B. H. M., "Advanced Propeller Performance Calculation by a Lifting Surface Method," *Journal of Propulsion and Power*, Vol. 12, No. 3, 1996, pp. 477–485.

[21]Schlichting, H., *Boundary Layer Theory*, McGraw–Hill, New York, 1979, Chap. 24.

[22]Kerschen, E. J., and Reba, R. A., "Active Control of Wake-Airfoil Interaction Noise by Leading Edge Actuators," *Proceedings of the 1st Joint CEAS/AIAA Aeroacoustics Conference* (Munich, Germany), Vol. 1, Deutsche Gesellschaft fuer Luft- und Raumfahrt, Bonn, Germany, 1995, pp. 435–444.

[23]Woodward, R. P., Bock, L. A., Heidelberg, L. J., and Hall, D. G., "Far-Field Noise and Internal Modes from a Ducted Propeller at Simulated Takeoff Conditions," AIAA Paper 92-0371, Jan. 1992.

S. Glegg
Associate Editor